

Experimental study on the mechanical property of coal and its application

Ting T. Jiang^a, Jian H. Zhang^{*}, Gang Huang^b, Shao X. Song^c and Hao Wu^{**}

Hubei Province Key Laboratory of Processing of Mineral Resources and Environment, School of Resource and Environmental Engineering, Wuhan University of Technology, Luoshi road No. 122, Wuhan 430070, Hubei, People's Republic of China

(Received February 14, 2017, Revised April 20, 2017, Accepted May 15, 2017)

Abstract. Brazilian splitting tests, uniaxial compression tests and triaxial compression tests are carried out on the coal samples cored from Shanxi group II₁ coal seam of Jiaozuo coal mine, Henan province, China, to obtain their property parameters. Considering the bedding has notable effect on the property parameter of coal, the samples with different bedding angles are prepared. The effects of bedding on the anisotropic characteristics of the coal seam are investigated. A geological geomechanical model is built based on the geology characteristics of the Jiaozuo coal mine target reservoir to study the effects of bedding on the fracture propagations during hydraulic fracturing. The effects of injection pressure, well completion method, in-situ stress difference coefficient, and fracturing fluid displacement on the fracture propagations are investigated. Results show bedding has notable effects on the property parameters of coal, which is the key factor affecting the anisotropy of coal. The hydraulic cracks trends to bifurcate and swerve at the bedding due to its low strength. Induced fractures are produced easily at the locations around the bedding. The bedding is beneficial to form a complicated fracture network. Experimental and numerical simulations can help to understand the effects of bedding on hydraulic fracturing in coalbed methane reservoirs.

Keywords: coal seam; coalbed methane; hydraulic fracturing; mechanical test; geomechanical model

1. Introduction

Precisely obtaining the mechanical parameters of the coal seam is a prerequisite to predict the fracture extension during hydraulic fracturing in CBM reservoirs (Chen *et al.* 2016, Damjanac *et al.* 2016, Sherwood *et al.* 2016). Due to the many joints, bedding, and tiny fractures in coal seams (Han *et al.* 2010), the property parameters of the coal from different locations are very different. Moreover, bedding is a main component with a random distribution in the coal, e.g., horizontal, wavy, and inclined orientations (Ganda *et al.* 2015, Zhao *et al.* 2016). These factors cause the typical anisotropy of coal seams and the property parameters of the coal to have a bedding direction characteristic. Therefore, fully understanding the effects of bedding on the coal seam property parameters is of great significance to understand the propagation rules of hydraulic fractures in CBM reservoir (Pan *et al.* 2014, Yoshimoto *et al.* 2016).

Several theoretical and experimental studies have been carried out to investigate the effect of coal seam mechanical properties on the fracture propagation during hydraulic

fracturing in coal seams. Thiercelin *et al.* (1989) proposed fracture toughness had significant effect on hydraulic fractures propagation and fracture network geometry. Gu *et al.* (2008) showed the in-situ stress was the dominant factor affecting the fracture height and Young's modulus had significant implications on fracture geometry and proppant placement. Yuan *et al.* (2012) researched the effect of injection pressure and elastic modulus of coal on fracture length and width. They proposed that fracture length increased linearly and the widest width varied exponentially with increasing injection pressure, while they both decreased linearly with the increase of Young's modulus. Wu *et al.* (2013) studied the effect of differential stress, elastic modulus, Poisson's ratio and pumping rate on the dimensions of a hydraulic fracture. They argued that the fracture height could be larger if the elastic modulus, Poisson's ratio and pumping rate were higher. Pan *et al.* (2013) and Wang *et al.* (2015) investigated the coal mechanical behaviors and macro-fracture density, P-wave velocity, porosity and permeability of different coal rank samples by using the experimental tests, and gave a quantitative relationship between P-wave velocity and permeability. Chong *et al.* (2014) comprehensively investigated the effect of formation mechanical properties (horizontal differential stress and matrix permeability) and fracturing fluid viscosity on the geometry of the hydraulic fracture network. They showed that the mechanical properties of the stratum had great influence on the fracture propagation. Song *et al.* (2014) indicated that the intersecting angle between coal-rock interface and horizontal profile, minimum horizontal in-situ stress, horizontal stress difference, elastic modulus difference and cohesive strength of coal-rock interface were the key factors

*Corresponding author, Professor
E-mail: zjhwut@sina.com

**Corresponding author, Professor
E-mail: haowu1977@163.com

^aPh.D.
E-mail: jiangtingting104@163.com

^bPh.D.
E-mail: huanggang1029@126.com

^cProfessor
E-mail: ssx851215@hotmail.com

affecting the fracture propagation direction. Heng *et al.* (2015) studied the effects of the orientations of bedding plane on shear strength and failure mechanisms. They proposed that there were three different failure modes when the bedding angles were different. Zhang *et al.* (2015) analyzed the effect of formation properties on the fracture propagation. They argued that it was beneficial to form a complex fracture network system if the horizontal stress difference was low, and the density of natural fractures had a great influence only on the condition of a low horizontal stress difference. Lu *et al.* (2015) confirmed that the hydraulic fracture tended to propagate along the coal-rock interface when fracture toughness of coal was low and elasticity modulus difference between coal bed and roof strata was high. However, achievements mentioned above were mainly based on the assumption that the coal seam was homogeneous without considering the effects of bedding. Jiang *et al.* (2016) and Grasselli *et al.* (2015) showed that the bedding had a significant influence on hydraulic fracture geometry.

Brazilian splitting tests and uniaxial and triaxial compression tests have been carried out on samples cored from Shanxi group II₁ coal seam of Jiaozuo coal mine, Henan province, China. The mechanical properties are obtained and the effects of bedding on the anisotropic characteristics of the coal seam are investigated. To study the effects of bedding on the hydraulic fracturing, a geological geomechanical model based on the target reservoir geology characteristics is developed by using RFPA software (Realistic Failure Process Analysis) (Tang *et al.* 2010). The propagation rules of the cracks and the influence of bedding on the fracture network in CBM reservoir are analyzed. Research results can provide a reference to understand the important role of bedding in forming the network cracks in CBM reservoirs during hydraulic fracturing.

2. Laboratory tests

2.1 Collection and preparation of coal samples

All the coal samples are taken from the Shanxi group II₁ coal seam in Jiaozuo coal mine of Henan province, China. Jiaozuo coal mining area belongs to a typical north China carboniferous-Permian coal-bearing stratum. The coal seam has large thickness (the average thickness is about 9 m), simple structure and distributional stability. Its depth is about -1070 m to -1080 m. The angle between bedding and the horizontal plane ranges from 18 to 35°.

To study the influence of bedding on coal rock mechanical parameters and predict the micro fractures propagation process, we carried out Brazilian splitting tests, uniaxial and triaxial compression tests. Water cutting is used to core samples from raw coal blocks. Due to the development of fractures in coal rock, the drilling speed is decreased to as low as possible to reduce the disturbance of the core samples during coring. The samples are polished to meet the requirements of test standards (Standard for tests method of engineering rock mass GB/T 50266-99 (1999); Specifications for rock tests in water conservancy and

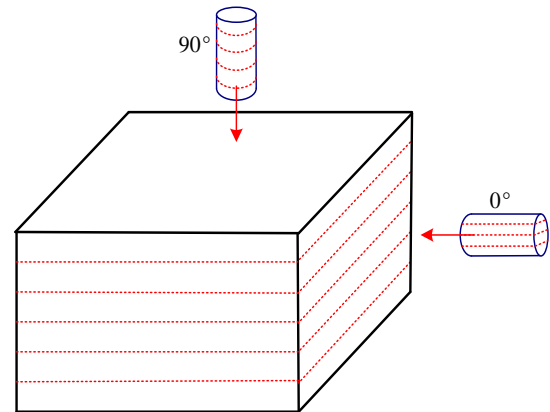


Fig. 1 Directional coring schematic diagram

hydroelectric engineering SL264-2001 (2010)). Because the raw coal is soft, the specimens are easily broken during coring. Through many coring tests, the angles between drilling direction and bedding plane are selected as 0° and 90° to ensure the integrity of the coal samples. Fig. 1 is a schematic diagram of the directional coring. The red dashed line indicates bedding.

The samples used in the tests are cylinder. The diameter and height of the samples for the uniaxial and triaxial compression tests are 50 mm and 100 mm, while that of the samples for the Brazilian splitting test samples are 50 mm and 25 mm, respectively. The machining error of all the samples are catered to the requirements of Standard for tests method of engineering rock mass GB/T 50266-99 (1999) and Specifications for rock tests in water conservancy and hydroelectric engineering SL264-2001 (2010).

2.2 Testing system

A multi-functional rock testing system (RMT) is used to carry out Brazilian splitting tests, uniaxial and triaxial compression tests on coal specimens with different bedding angles. The rock testing system is controlled by computer through the whole course. It has a multi-channel data acquisition system with high testing precision and stable system performance. Its maximum axial load is 1000 kN and the piston displacement is 0-50 mm. The confining pressure range is 0-50 MPa, and the confining pressure rate is 0.001-1 MPa/s. The deformation rate is 0.0001-1 mm/s and the loading rate is 0.01-100 kN/s. Its fatigue frequency is 0.001-1 kHz, and the housing rigidity is 5×10^6 N/mm (Jiang *et al.* 2017).

2.3 Brazilian splitting tests

Fig. 2 presents the schematic diagram of Brazilian disk splitting test. To obtain the tensile strength of the matrix and bedding separately, the samples are divided into two groups. One group is the disk plane parallel to bedding (Fig. 2(a)), and the other group is the disk plane perpendicular to bedding (Fig. 2(b)). As shown in Fig. 2(b), bedding angle is defined as the angle between bedding and loading direction. The axial displacement control mode is used with a value of 0.002 mm/s (Chen *et al.* 2016). When the samples fail, tests

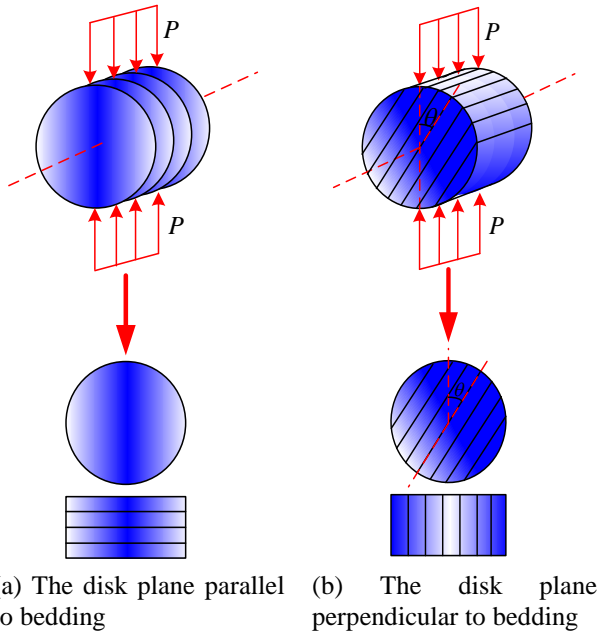


Fig. 2 Schematic diagram of Brazilian disk splitting test (θ is the bedding angle)

Table 1 Brazilian splitting test results

| Bedding direction | Bedding angle ($^{\circ}$) | Tensile strength (MPa) |
|-----------------------|------------------------------|------------------------|
| Parallel to disk | 180 | 1.17 |
| Perpendicular to disk | 90 | 0.54 |
| Perpendicular to disk | 0 | 0.27 |



Fig. 3 Splitting failure pattern (Sample diameter=50 mm)

stop. To reduce the errors, tests under the same conditions are repeated at least three times, and the average values are calculated as the tensile strength used in the numerical simulations.

Brazilian splitting test results are listed in Table 1. When the disk plane is parallel to the bedding (bedding angle=180 $^{\circ}$), the tensile strength is 1.17 MPa, which is the largest. It shows the matrix has the maximum tensile strength. When the bedding angle is 0 $^{\circ}$, the tensile strength is the smallest (0.27 MPa). It reveals that bedding is a weak interface of CBM reservoir. When the bedding angle is 90 $^{\circ}$, the tensile strength increases to about 0.54 MPa, which is about two times of that of the bedding angle is 0 $^{\circ}$. It shows the bedding has notable effect on the tensile strength of coal rock. The test results also show the tensile strength of coal

rock has the anisotropy characteristics.

Brazilian fracture shapes are shown in Fig. 3. When the bedding angle is 180 $^{\circ}$ (Fig. 3(a)), the main fracture goes through the disk center line extends along the loading direction. Local bifurcation cracks develop near the loading point with a small length. This is mainly caused by the stress concentration. For this condition, the measured tensile strength is the tensile strength of the matrix and has the maximum value. When the bedding angle is 90 $^{\circ}$ (Fig. 3(b)), the main fracture approximately passes through the center line of the disk and extends vertically to the bedding. Due to the strength difference between the matrix and bedding, a horizontal secondary crack along the bedding direction is formed. A tilted branch crack is generated at the center of the disk, and finally a complex fracture is formed. Because the major fracture approximately passes through the center of the disk, the rupture strength approximates the tensile strength perpendicular to bedding. When bedding angle is 0 $^{\circ}$, the vertical crack extends through the center line of the sample along bedding to form a relatively flat fracture (Fig. 3(c)). So the obtained strength is the tensile strength of the bedding, which is the minimum value. The results also show when the bedding angle is 0 $^{\circ}$, there is only one main fracture without secondary branch fractures (Fig. 3(c)). It is because the strength of the bedding is much smaller than that of the matrix, and the failure firstly takes place along the bedding. When the bedding angle is 180 $^{\circ}$, a secondary branch fracture appears which locates at the edge of the sample (Fig. 3(c)). The sample is composed of the matrix and has a good homogeneity. The secondary branch fracture may be caused by the stress concentration at the loading points. When the bedding angle is 90 $^{\circ}$, the sample is composed of the bedding and matrix, and they are perpendicular. Due to the loads are subjected to the matrix, the fracture firstly appears in the matrix. When the fracture propagates a distance about 1/2 sample diameter, a secondary fracture appears along the bedding. It has an angle with main fracture about 45 $^{\circ}$ and a length of about 25 mm. This may be caused by the shear failure of the bedding.

The failure mechanism of Brazilian splitting tests can be divided into two types, which are strongly affected by the direction of bedding. When the bedding parallels the disk plane, the failure of coal samples is mainly controlled by the tensile strength of the matrix. Then the bedding has no obvious influence on the splitting failure of coal rock. When the bedding is perpendicular to the disk and the bedding angle is 0 $^{\circ}$, the tensile splitting occurs along the bedding. The failure is mainly controlled by the bedding. When the bedding angle is 90 $^{\circ}$, the coal samples show the tensile failure both through and along the bedding. The failure is controlled by the matrix and the bedding. In conclusion, the bedding is the main reason leading to the anisotropy of failure pattern and rupture mechanism.

2.4 Uniaxial compression tests

The samples are divided into two groups based on the orientation of bedding vs. axial load. In one group the angle between the long axis of the sample and the bedding is equal to 0 $^{\circ}$, and that of the other group is 90 $^{\circ}$. Each

Table 2 Uniaxial compression test results

| | Bedding angle (°) | Sample size (mm) | | Compressive strength (MPa) | Elasticity modulus (GPa) | Poisson's ratio |
|---------------|-------------------|------------------|--------|----------------------------|--------------------------|-----------------|
| | | Diameter | Height | | | |
| Average value | 0 | 49.76 | 99.76 | 3.06 | 0.65 | 0.34 |
| Average value | 90 | 49.68 | 99.71 | 11.88 | 1.93 | 0.31 |



(i) Before test (ii) After test (i) Before test (ii) After test
(a) Bedding angle 0° (b) Bedding angle 90°

Fig. 4 Samples before and after uniaxial compression

Table 3 Triaxial compression test results when bedding angle is 0°

| | Diameter (mm) | Height (mm) | Confining pressure (MPa) | Axial stress at failure (MPa) |
|---------------|---------------|-------------|--------------------------|-------------------------------|
| Average value | 49.57 | 99.61 | 1 | 6.331 |
| Average value | 49.65 | 99.64 | 2 | 11.572 |
| Average value | 49.78 | 99.83 | 3 | 15.726 |
| Average value | 49.68 | 99.65 | 4 | 19.218 |
| Average value | 49.87 | 99.82 | 5 | 23.774 |

Table 4 Triaxial compression test results when bedding angle is 90°

| | Diameter (mm) | Height (mm) | Confining pressure (MPa) | Axial stress at failure (MPa) |
|---------------|---------------|-------------|--------------------------|-------------------------------|
| Average value | 49.58 | 99.69 | 1 | 15.314 |
| Average value | 49.82 | 99.75 | 2 | 19.358 |
| Average value | 50.01 | 99.71 | 3 | 23.458 |
| Average value | 49.79 | 99.78 | 4 | 26.054 |
| Average value | 49.82 | 99.75 | 5 | 29.406 |

configuration of tests is performed on at least three samples, and we take the average of the test results. Cylindrical specimens are placed in a rubber sleeve before loading to keep the broken samples with relatively intact shapes after the tests (Chen *et al.* 2015). When the deformation sensor and signal receiver are connected, we preload the specimen. We adopt displacement-control mode and the loading rate is kept at 0.002 mm/s until the specimen fails (Fan *et al.* 2017).

Table 2 lists the test results of uniaxial compression. It shows the compressive strength and elastic modulus of coal rocks are affected by the angle between coring direction and bedding plane greatly. Compressive strength of the sample with a bedding angle of 90° (11.88 MPa) is much larger than that with a bedding angle of 0° (3.06 MPa). However, Poisson's ratio is slightly affected by the angle between

coring direction and bedding plane.

Fig. 4 shows typical failure patterns for different bedding angles. When the bedding angle is 0°, tensile fracturing takes place along the bedding with multiple tension fracture planes parallel to the bedding, and a breakthrough on both ends. When the bedding angle is 90°, samples show complex tension splitting and shear failures, and the samples easily break into pieces.

The failure mechanism of coal samples under uniaxial compression is classified into two types: (1) Tensile splitting failure occurs along bedding when the bedding angle is 0°, and the failure is mainly controlled by the bedding. (2) The complicated tensile splitting and shear failure both take place with the bedding angle of 90°, and the failure is mainly controlled by the matrix.

2.5 Triaxial compression tests

During the triaxial compression tests, the axial loads are controlled by the axial displacement control mode. The loading rate is 0.002 mm/s. Confining pressure is increased to the predetermined value at a rate of 0.1 MPa/s. Then axial load is applied until the sample fails.

The bedding angles remain 0° and 90° and the confining pressures are 1, 2, 3, 4, and 5 MPa. Each group under the same confining pressure consists of at least three samples, and then we take the average of the experimental results.

Tables 3 and 4 show the test results of triaxial compression for different bedding angles.

The test results show that the compressive strength and the elastic modulus under triaxial compression have significant anisotropy. Fig. 5 shows the relationship between compressive strength and confining pressure at different bedding angles.

When the bedding angle is 0°, the regression relationship of compressive strength and confining pressure can be written as

$$\sigma_{tc,0^\circ} = 4.182\sigma_3 + 2.824 \quad (1)$$

$$R^2 = 0.99634 \quad (2)$$

where $\sigma_{tc,0^\circ}$ is the compressive strength when bedding angle is 0°, Pa; σ_3 is the confining pressure, Pa; R^2 is the determination coefficient.

When the bedding angle is 90°, the regression relationship of compressive strength and confining pressure is shown as follows

$$\sigma_{tc,90^\circ} = 3.54\sigma_3 + 12.058 \quad (3)$$

$$R^2 = 0.99478 \quad (4)$$

where $\sigma_{tc,90^\circ}$ is the compressive strength when bedding angle is 90°, Pa.

As shown in Fig. 5, the triaxial compressive strength increases significantly with increasing confining pressure, and has good correlation, with linear relationships. Two reasons explain these phenomena: (1) The axial load produces lateral deformation and the confining pressure opposes to it. (2) There are a large number of cracks in the coal sample, and the frictional force has a great influence on

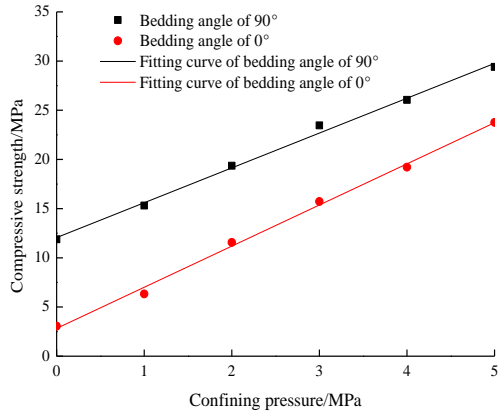
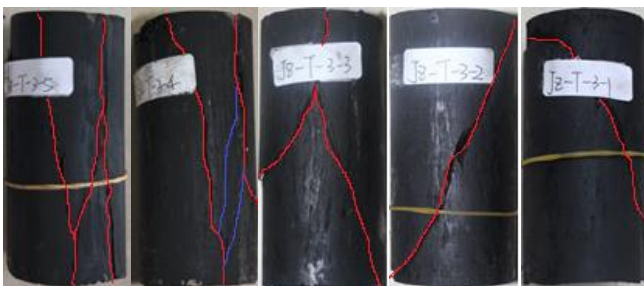
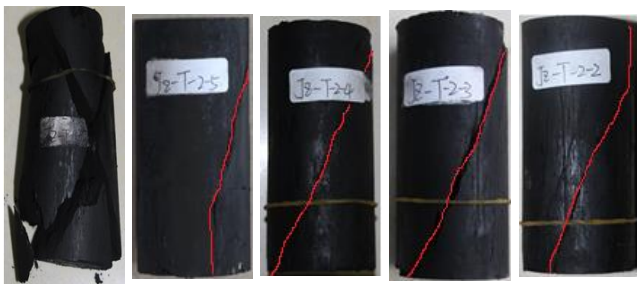


Fig. 5 The curve between compressive strength and confining pressure



(a) 1 MPa (b) 2 MPa (c) 3 MPa (d) 4 MPa (e) 5 MPa

Fig. 6 Coal triaxial compression fracturing geometries of bedding angle 0°



(a) 1 MPa (b) 2 MPa (c) 3 MPa (d) 4 MPa (e) 5 MPa

Fig. 7 Coal triaxial compression fracturing geometries of bedding angle 90°

Table 5 Coal rock triaxial compression angle of internal friction and cohesion

| | Internal friction angle (°) | Cohesive strength (MPa) |
|---------|-----------------------------|-------------------------|
| Matrix | 18.8 | 0.82 |
| Bedding | 16.3 | 0.19 |

the deformation. Increasing the confining pressure increases the normal stress on the crack surfaces, and the frictional strength increases accordingly. Ultimately, it restrains the slipping deformation along the fissure surfaces.

Figs. 6 and 7 show typical fracture styles of the samples with different bedding angles under the triaxial compression. With increasing confining pressure, fracturing energy increases until the peak axial stress is reached. The energy released by the elastic deformation becomes much

smaller than the fracturing energy needed to form cracks when the confining pressure is increased. This means that the released elastic energy is insufficient to induce further damage, and coal dynamic damage is reduced. Coal specimens rupture mode basically shows the following two types of failure: (1) Conjugate shear failure. Two or more fracture planes develop in the samples, which can be divided into two groups parallel to each other. The two groups of failure surfaces cross through the sample and the broken sample is divided into several pieces, eventually a conjugate shear fracture surface is formed. The failure mode is of this kind (JZ-T-3-5 and JZ-T-3-4) when confining pressures are 1 MPa and 2 MPa with bedding angle 0°. (2) Single shear failure. Destroyed specimens all have one or two primary shear surfaces which generally go through both ends of the samples. When bedding angle is 90° or confining pressure is higher (>2 MPa), a single shear failure develops. It is mainly because the strength of the sample is determined by the matrix. Due to the effects of confining pressure, the influence of bedding on sample failure mode decreases seriously comparing with the uniaxial compression failure. As the increase of confining pressure, the damage form is no longer splitting failure, but shear failure.

According to Mohr-Coulomb strength theory, the triaxial compression characteristic parameters of matrix and bedding are determined and are shown in Table 5.

In conclusion, the tensile strength, compressive strength, elasticity modulus and cohesive strength of bedding are the minimum in coal rock. When the fracture propagates perpendicularly to the bedding, it is most likely to bifurcate and turn around at the bedding plane to produce induced fractures. It can form complex fracture morphology, which is a benefit for fracturing transformation in coal gas reservoirs.

3. Numerical simulation of hydraulic fracture propagation

Due to the notable property variations of the coal seam, it is nearly impossible to prepare samples from the raw coal to study the effects of a given parameter (such as completion method and fracture toughness) on the hydraulic fracturing. However, the effects of these parameters on the hydraulic fracturing are useful for the actual design of a CBM well. To investigate the effects of the parameters, a geological geomechanical model of hydraulic fracturing of a vertical well in a coal seam was constructed. According to the physical tests, the bedding has notable effects on the hydraulic fracturing in coal seams. Therefore, the bedding is included in the numerical model. The coupling of stress, seepage and damage are considered during simulating the crack propagation. The reservoir geologic parameters were obtained from No.2 coal seam in Jiaozuo mining area. The results can provide a reference basis for the fracture propagation rule and the geometry of fracture network of CBM reservoirs.

3.1 Coupling equations

To show different mechanical properties at different

locations, the Weibull statistical distribution function (Dalian Mechsoft Co., Ltd 2011) is introduced to describe the mechanical property distribution of the discrete mesoscopic unit

$$\varphi(\alpha) = \frac{m}{\alpha_0} \cdot \left(\frac{\alpha}{\alpha_0}\right)^{m-1} \cdot e^{-\left(\frac{\alpha}{\alpha_0}\right)^m} \quad (5)$$

where α is the physical mechanical parameter of rock unit; α_0 stands for the average value of the physical mechanical parameter of rock unit; m is homogeneity coefficient; $\varphi(\alpha)$ is statistical distribution density of α .

We assume that the fluid flow in the rock follows Biot seepage theory, then the basic equations on seepage-stress coupling can be written as

$$\sigma_{ij,j} + \rho X_j = 0 \quad (i, j = 1, 2, 3) \quad (6)$$

$$\varepsilon_{ij} = \frac{1}{2}(u_{i,j} + u_{j,i}) \quad (7)$$

$$\varepsilon_v = \varepsilon_{11} + \varepsilon_{22} + \varepsilon_{33} \quad (8)$$

$$\sigma'_{ij} = \sigma_{ij} - \alpha p \delta_{ij} = \lambda \delta_{ij} \varepsilon_v + 2G \varepsilon_{ij} \quad (9)$$

$$K \nabla^2 p = \frac{1}{Q} \frac{\partial p}{\partial t} - \alpha \frac{\partial \varepsilon_v}{\partial t} \quad (10)$$

where σ_{ij} is normal stress, Pa; ρ is volume force density, N/m³; ε_{ij} is normal strain; ε_v is volume strain; u stands for displacement component, m; α is pore pressure coefficient; p is pore water pressure, Pa; λ is Lamé constant; δ is Kronecker coefficient; K is permeability coefficient, m/s; ∇^2 is Laplace operator; Q is Biot coefficient.

In this paper, the solid is considered as a porous medium. The coupling equation of permeability coefficient and damage is shown as below

$$K = \begin{cases} K_0 e^{-\beta(\sigma_3 - \alpha p)} & D = 0 \\ \xi K_0 e^{-\beta(\sigma_3 - \alpha p)} & 0 < D < 1 \\ \xi' K_0 e^{-\beta(\sigma_3 - \alpha p)} & D = 1 \end{cases} \quad (11)$$

where K_0 is the initial permeability coefficient, m/s; β is coupling coefficient; D is damage variable; ξ' and ξ stand for the coefficients related to the permeability.

3.2 Numerical simulation model

The numerical simulation model is built by finite element software RFPA (Tang *et al.* 2010). The model and its boundaries are shown in Fig. 8. We take the cross section perpendicular to the wellbore as the research object to establish the calculation model of a well with perforation completion, and ignore the impact of the casing and the cement sheath on fracturing effect due to the hydraulic fracturing in CBM reservoir being the study target. It is a square with the side length of 10 m, and the wellbore diameter is about 0.2 m (in order to better display the confining pressure in wellbore, the wellbore dimension is enlarged in Fig. 8). To eliminate the boundary effect on the calculating results, the distance between the wellbore and the boundary is more than 10 times larger than the wellbore

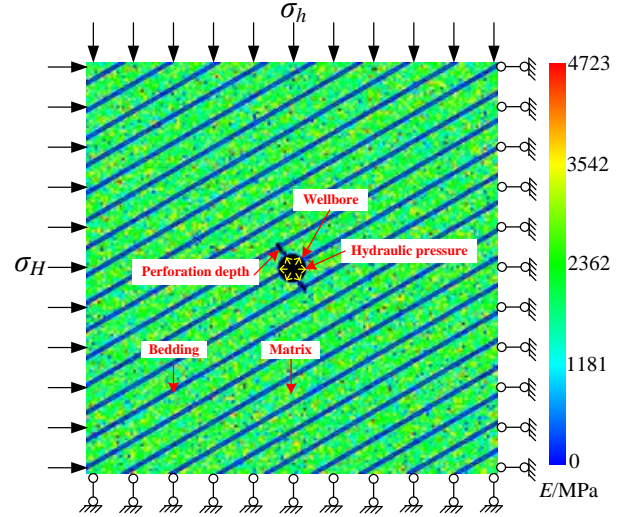


Fig. 8 Numerical model and its boundaries

Table 6 Parameters used in the simulation model

| No. | Items | Unit | Matrix | Bedding |
|-----|---------------------------|----------------------|--------|---------|
| 1 | Poisson's ratio | | 0.31 | 0.34 |
| 2 | Internal friction angle | degree | 18.8 | 16.3 |
| 3 | Elasticity modulus | GPa | 1.93 | 0.65 |
| 4 | Tensile strength | MPa | 1.17 | 0.27 |
| 5 | Cohesive strength | MPa | 0.82 | 0.19 |
| 6 | Permeability | mD | 0.154 | 1.644 |
| 7 | Porosity | % | 4.8 | 3.8 |
| 8 | Compressive strength | MPa | 11.88 | 3.06 |
| 9 | Fracture toughness | MPa m ^{0.5} | 0.364 | 0.12 |
| 10 | Vertical stress | MPa | 23.4 | |
| 11 | Maximum horizontal stress | MPa | 25.7 | |
| 12 | Minimum horizontal stress | MPa | 16.7 | |

diameter. There are 300×300 elements in the model, and the perforation depth is 150 mm with a direction perpendicular to the bedding. The horizontal in-situ stresses are applied on two sides of the model, and the displacement boundary is applied on the other two sides. The bedding has darker color and narrower scope, as also marked in Fig. 8. According to the actual geological data, the angle between the bedding and the horizontal plane is 18-35°. In order to simplify the calculation, the angle is valued as 30° in the numerical simulations.

The hydraulic pressure is increased at a rate of 0.1 MPa by single-step until the stratum ruptures completely to form a certain number of hydraulic fracture channels. The fracturing fluid is water with the density and the displacement of 1000 kg/m³ and 0.5 ml/s, respectively. Table 6 lists the parameters used in the numerical simulation.

3.3 Simulation results and analysis

Fig. 9 presents the hydraulic fractures evolution in the CBM reservoir when the injection pressures are simulated

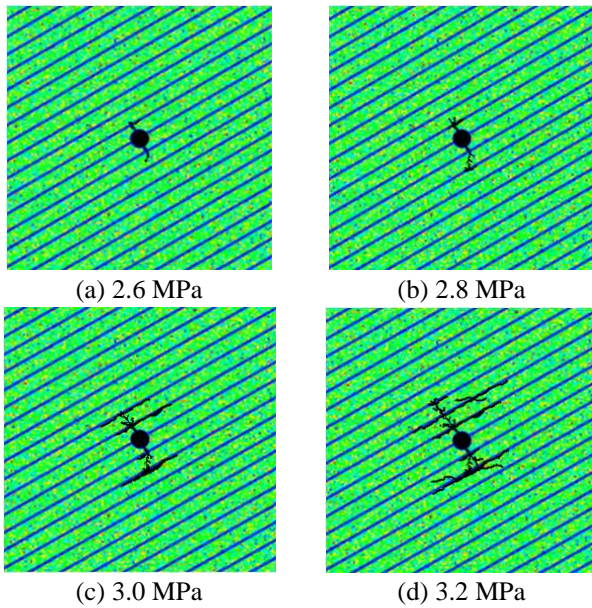


Fig. 9 Hydraulic fractures evolution for different injection pressures

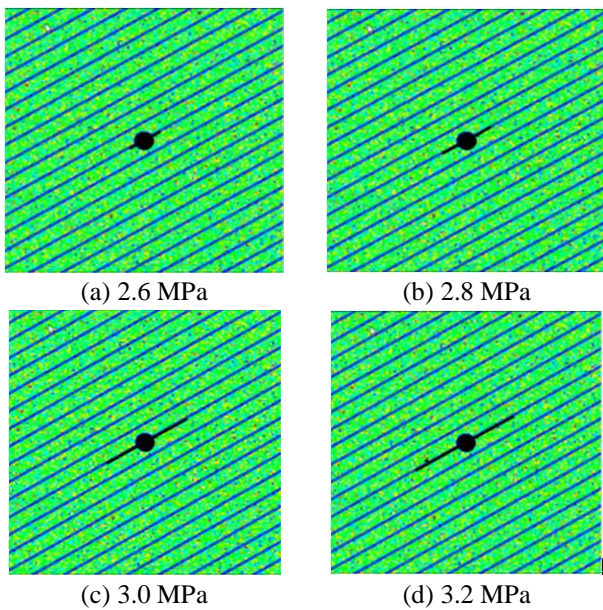


Fig. 10 Hydraulic fracture evolution plot on barefoot well completion

as 2.6 MPa, 2.8 MPa, 3.0 MPa and 3.2 MPa. The fractures firstly appear at the ends of the perforation and then propagate along the perforating direction (Fig. 9(a)). As the fracturing fluid being injected into the formation continuously, the fractures extend to the bedding, and take place bifurcation and diversion for the low strength and high permeability of the bedding (Fig. 9(b)). Many secondary fractures are produced in the bedding, while the main fracture still propagates perpendicularly to the bedding. However, the fracture propagation speed decreases greatly due to these secondary fractures consume much energy carried by the fracturing fluid.

When the major and secondary fractures extend to a certain distance along the bedding, the energy carried by the

fracturing fluid cannot maintain the rapid extension of the cracks. The lengths of the cracks are not increased. So the new secondary cracks are formed along another bedding. However, the newly formed cracks cannot stop the continuous extension of the major fracture and the original induced fractures completely but reduces their extension speed (Fig. 9(c)). Ultimately, a complex hydraulic fracture network is formed, which will keep stable until the displacement is increased. And then, some new major and secondary fractures are formed to reach a new balance (Fig. 9(d)). Therefore, intermittent increase displacement of fracturing fluid is proposed for the hydraulic fracturing of CBM reservoirs.

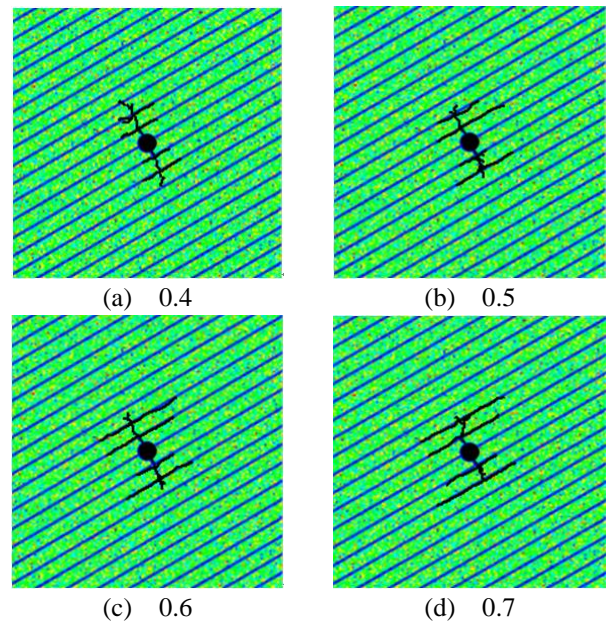


Fig. 11 Hydraulic fracture geometry on different in-situ stress difference coefficients

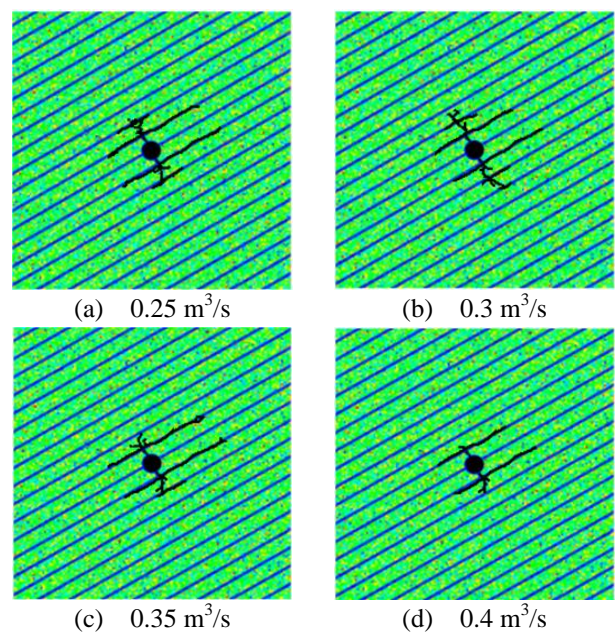


Fig. 12 Hydraulic fracture geometry on different fracturing fluid displacements

3.4 Analysis on influence factor of hydraulic fracture geometry

3.4.1 Completion method

The fracture morphology evolution procedure of open hole completion is shown in Fig. 10. Although the bedding is not parallel with the horizontal maximum principal stress, the hydraulic fracture still initiates along the bedding. The hydraulic fracture propagates along the bedding with increasing fracturing fluid and the extension path is relatively smooth. Finally, a single fracture along the bedding is formed in the coal seam.

To further analyze the effect of in-situ stress difference coefficient and fracturing fluid displacement on hydraulic fracture geometry can deepen the understanding of the formation mechanism of fracture network during hydraulic fracturing under the condition of perforation completion.

3.4.2 In-situ stress difference coefficient

The in-situ stress difference coefficient is shown as below

$$k = (\sigma_H - \sigma_h) / \sigma_h \quad (12)$$

where σ_H is the maximum horizontal principal stress, Pa; σ_h is the minimum horizontal principal stress, Pa.

Keeping other parameters constant, we only change the maximum horizontal principal stress to analyze the influence rule of different in-situ stress difference coefficient on hydraulic fracture geometry. When the stress difference coefficients are 0.4, 0.5, 0.6 and 0.7, the hydraulic fracture geometries are shown in Fig. 11.

Known from Fig. 11, the differences of hydraulic fractures are mainly reflects on two aspects: the propagation length of major fracture along perforation direction and the extend length of induced fractures along bedding. When the in-situ stress difference coefficient is small, the major fracture tends to extend along the perforation direction. The propagation distance of major fracture is far while the extension lengths of secondary fractures are small. When the in-situ stress difference coefficient is larger, the energy needed to propagate along the perforation direction by major fracture is higher. So the propagation distance of major fracture is short, the secondary fractures are more likely to extend along bedding with higher extension distance.

3.4.3 Fracturing fluid displacement

The hydraulic fracture geometries of different fracturing fluid displacements (0.25, 0.3, 0.35 and 0.4 m³/s) are shown in Fig. 12. Fracturing fluid displacement has great effect on hydraulic fracture geometry. When the fracturing fluid displacement is low (Fig. 12(a) and 12(b)), the hydraulic fracture tends to propagate vertical to the bedding. The major fracture has a number of bifurcation and diversion at the bedding to form several induced fractures which propagate along the bedding. With the increase of the displacement (Fig. 12(c) and 12(d)), the number of bifurcation and diversion at the bedding of hydraulic fractures decreases and the number of secondary cracks also reduces gradually. However, the propagation lengths of

secondary fractures along bedding are increased. It means the fracture geometry is more complicated on the condition of low fracturing fluid displacement, while the fracture morphology is relatively simple under the high displacement condition.

Comparing Fig. 12(a) and 12(b), the fracturing fluid displacement should not to be too small which is not beneficial for the rapid extension of hydraulic fracture. Therefore, we should control the fracturing fluid displacement timely during hydraulic fracturing of coal seam. This not only promotes the bifurcation and diversion of the major fracture at the bedding to form a number of secondary cracks, but also controls their propagation speed to form the fracture network.

4. Conclusions

- The Brazilian splitting tensile strength of coal rock shows prominent directionality. It is mainly because the tensile strength of the bedding is much smaller than that of the matrix. The compressive strength and elastic modulus of coal show strong anisotropic characteristic, while the difference of Poisson's ratio is small. The failure mode of coal specimens is typical brittle failure. The triaxial compressive strength increases significantly with an increasing confining pressure and shows a linear relationship. The anisotropy of coal rock fracturing mode is closely related to the bedding angle and confining pressure. As the increase of the confining pressure, the effect of bedding on failure becomes indistinctive and the samples mainly fail in shear.

- Numerical simulations show the hydraulic fracture initiates at the end of the perforation due to tension fracturing, and it generates the induced fractures at the bedding. The propagation speed of secondary fractures is much faster than that of the major fracture. The bifurcation and diversion of major fracture takes place at the bedding during the fracture further extension process. Bedding is beneficial to create complicated fracture network which achieves the purpose of CBM reservoir fracturing treatment.

- A single crack is formed in coal seam on open hole completion. It is more likely to form complicated fracture network on the condition of perforation completion to improve the effect of hydraulic fracturing. The in-situ stress difference coefficient has little influence on hydraulic fracture geometry and the geometry shows great similarity. The fracturing fluid displacement has great effect on the fracture geometry. To control the fracturing fluid displacement timely is benefit on forming complex fracture network.

Acknowledgements

This paper was funded by the China Postdoctoral Science Foundation Funded Project (No. 2016M592402), Hubei Provincial Natural Science Foundation of China (Nos. 2016AHB015, 2016CFA013), and Wuhan Science and Technology Bureau (No. 2016070204020156).

References

- Chen, J., Du, C., Jiang, D.Y., Fan, J.Y. and He, Y. (2016), "The mechanical properties of rock salt under cyclic loading-unloading experiments", *Geomech. Eng.*, **10**(3), 325-334.
- Chen, J., Yin, L., Ren, S., Lin, L. and Fang, J. (2015), "The thermal damage properties of mudstone, gypsum and rock salt from Yingcheng, Hubei, China", *Minerals*, **5**(1), 104-116.
- Chong, H.A., Robert, D. and John, Y.W. (2014), "Development of innovative and efficient hydraulic fracturing numerical simulation model and parametric studies in unconventional naturally fractured reservoirs", *J. Unconv. Oil Gas Resour.*, **8**, 25-45.
- Dalian Mechsoft Co., Ltd (2011), *Realistic Failure Process Analysis: Users Guide*.
- Damjanac, B. and Cundall, P. (2016), "Application of distinct element methods to simulation of hydraulic fracturing in naturally fractured reservoirs", *Comput. Geotech.*, **71**, 283-294.
- Fan, J., Chen, J., Jiang, D., Chemenda, A., Chen, J. and Ambre, J. (2017), "Discontinuous cyclic loading tests of salt with acoustic emission monitoring", *J. Fatigue*, **94**, 140-144.
- Ganda, M.S. and Sugeng, W. (2015), "Effect of bedding plane on prediction blast-induced ground vibration in open pit coal mines", *J. Rock Mech. Min. Sci.*, **79**, 1-8.
- Grasselli, G., Lisjak, A., Mahabadi, O.K. and Tatone, B.S.A. (2015), "Influence of pre-existing discontinuities and bedding planes on hydraulic fracturing initiation", *Eur. J. Environ. Civ. Eng.*, **19**(5), 580-597.
- Gu, H.R. and Siebrits, E. (2008), "Effect of formation modulus contrast on hydraulic fracture height containment", *SPE Prod. Oper.*, **23**(2), 170-176.
- Han, F.S., Busch, A., Krooss, B.M., Liu, Z.Y., Wageningen, N.V. and Yang, J.L. (2010), "Experimental study on fluid transport processes in the cleat and matrix systems of coal", *Energy Fuel*, **24**(12), 6653-6661.
- Heng S., Guo Y.T., Yang, C.H., Daemen J.J.K. and Li, Z. (2015), "Experimental and theoretical study of the anisotropic properties of shale", *J. Rock Mech. Min. Sci.*, **74**, 58-68.
- Industry standard editorial committee of the People's Republic of China (2010), *Specifications for Rock Tests in Water Conservancy and Hydroelectric Engineering SL264-2001*, China Waterpower Press, Beijing, China.
- Jiang T.T., Zhang, J.H. and Wu, H. (2016), "Experimental and numerical study on hydraulic fracture propagation in coalbed methane reservoir", *J. Nat. Gas Sci. Eng.*, **35**, 455-467.
- Jiang T.T., Zhang, J.H. and Wu, H. (2017), "Impact analysis of multiple parameters on fracture formation during volume fracturing in coalbed methane reservoirs", *Curr. Sci.*, **112**(2), 332-347.
- Lu, Y.Y., Song, C.P., Jia, Y.Z., Xia, B.W., Ge, Z.L., Tang, J.R. and Li, Q. (2015), "Analysis and numerical simulation of hydrofracture crack propagation in coal-rock bed", *CMES Comput. Model. Eng. Sci.*, **105**(1), 69-86.
- Pan, J.N., Meng, Z.P., Hou, Q.L., Ju, Y.W. and Cao, Y.X. (2013), "Coal strength and Young's modulus related to coal rank, compressional velocity and maceral composition", *J. Struct. Geol.*, **54**, 129-135.
- Pan, J.N., Wang, H.C., Wang, K. and Niu, Q.H. (2014), "Relationship of fractures in coal with lithotype and thickness of coal lithotype", *Geomech. Eng.*, **6**(6), 613-624.
- Sherwood, O.A., Rogers, J.D., Lackey, G., Burke, T.L., Osborn, S.G. and Ryan, J.N. (2016), "Groundwater methane in relation to oil and gas development and shallow coal seams in the Denver-Julesburg basin of Colorado", *Proc. Natl. Acad. Sci. USA*, **113**(30), 8391-8396.
- Song, C.P., Lu, Y.Y., Jia, Y.Z. and Xia, B.W. (2014), "Effect of coal-rock interface on hydraulic fracturing propagation", *J. Northeast. Univ.*, **35**(9), 1340-1345 (in Chinese).
- State Bureau of Quality Technical Supervision, Ministry of Construction of the People's Republic of China (1999), *Standard for Tests Method of Engineering Rock Masses GB/T 50266-99*, China Planning Press, Beijing, China.
- Tang, C.A. and Hudson, J.A. (2010), *Rock Failure Mechanisms Explained and Illustrated*, CRC Press, Boca Raton, Florida, U.S.A.
- Thiercelin, M., Jeffrey, R.G. and Naceur, K.B. (1989), "Influence of fracture toughness on the geometry of hydraulic fractures", *Proceedings of the Low Permeability Reservoirs Symposium*, Denver, Colorado, U.S.A., May.
- Wang, H.C., Pan, J.N., Wang, S. and Zhu, H.T. (2015), "Relationship between macro-fracture density, p-wave velocity, and permeability of coal", *J. Appl. Geophys.*, **117**, 111-117.
- Wu, B.L., Cheng, Y.F., Li, Y.Z., Xu, P. and Zhang, Y.T. (2013), "Factor analysis of vertical hydraulic fracture geometry in coal bed", *Proceedings of the 2013 International Conference on Energy Engineering and Environmental Engineering*, Hangzhou, China, January.
- Yoshimoto, N., Wu, Y., Hyodo, M. and Nakata, Y. (2016), "Effect of relative density on the shear behaviour of granulated coal ash", *Geomech. Eng.*, **10**(2), 207-224.
- Yuan, Z.G., Wang, H.T., Liu, N.P. and Liu, J.C. (2012), "Simulation study of characteristics of hydraulic fracturing propagation of low permeability coal seam", *Disaster Adv.*, **5**(4), 717-720.
- Zhang, S.C., Lei, X., Zhou, Y.S. and Xu, G.Q. (2015), "Numerical simulation of hydraulic fracture propagation in tight oil reservoirs by volumetric fracturing", *Petrol. Sci.*, **12**(4), 674-682.
- Zhao, T.B., Guo, W.Y., Lu, C.P. and Zhao, G.M. (2016), "Failure characteristics of combined coal-rock with different interfacial angles", *Geomech. Eng.*, **11**(3), 345-359.

CC